Design, synthesis and biological activity of novel substituted 3-benzoic acid derivatives as *Mt*DHFR inhibitors

Thales Kronenberger, Glaucio Monteiro Ferreira, Alfredo Danilo Ferreira de Souza, Soraya da Silva Santos, Antti Poso, João Augusto Ribeiro, Maurício Temotheo Tavares, Fernando Rogério Pavan, Gustavo Henrique Goulart Trossini, Marcio Vinícius Bertacine Dias, Roberto Parise-Filho

PII: S0968-0896(20)30430-2
DOI: https://doi.org/10.1016/j.bmc.2020.115600
Reference: BMC 115600

To appear in: *Bioorganic & Medicinal Chemistry*

Received Date: 21 February 2020
Revised Date: 2 June 2020
Accepted Date: 16 June 2020

Please cite this article as: Kronenberger, T., Monteiro Ferreira, G., Danilo Ferreira de Souza, A., da Silva Santos, S., Poso, A., Augusto Ribeiro, J., Temotheo Tavares, M., Rogério Pavan, F., Henrique Goulart Trossini, G., Vinícius Bertacine Dias, M., Parise-Filho, R., Design, synthesis and biological activity of novel substituted 3-benzoic acid derivatives as *Mt*DHFR inhibitors, *Bioorganic & Medicinal Chemistry* (2020), doi: https://doi.org/10.1016/j.bmc.2020.115600

Design, synthesis and biological activity of novel substituted 3-benzoic acid derivatives as *Mt*DHFR inhibitors

Thales Kronenberger[a,b¥], Glaucio Monteiro Ferreira[c¥], Alfredo Danilo Ferreira de Souza[d¥], Soraya da Silva Santos[e], Antti Poso[a,b], João Augusto Ribeiro[f], Maurício Temotheo Tavares[d], Fernando Rogério Pavan[g], Gustavo Henrique Goulart Trossini[h], Marcio Vinícius Bertacine Dias[f,i], Roberto Parise-Filho[d*]

[a] Department of Oncology and Pneumonology, Internal Medicine VIII, University Hospital Tübingen, Otfried-Müller-Straße 10, DE 72076, Tübingen, Germany.
[b] School of Pharmacy, Faculty of Health Sciences, University of Eastern Finland, 70211 Kuopio, Finland.
[c] Laboratory of Molecular Biology applied to Diagnosis (LBMAD), Department of Pharmacy, Faculty of Pharmaceutical Sciences, University of São Paulo, São Paulo, SP, Brazil.
[d] Laboratory of Design and Synthesis of Bioactive Substances (LAPESSB), Faculty of Pharmaceutical Sciences, University of São Paulo, Prof. Lineu Prestes Avenue, 580, Bl.13, São Paulo, SP, Brazil.
[e] Laboratory of Design and Synthesis of Chemotherapeutics Potentially Active in Neglected Diseases (LAPEN), Department of Pharmacy, Faculty of Pharmaceutical Sciences, University of São Paulo, São Paulo, SP, Brazil.
[f] Department of Microbiology, Institute of Biomedical Sciences, University of São Paulo, São Paulo, SP, Brazil
[g] Department of Biological Sciences, School of Pharmaceutical Sciences, São Paulo State University, Araraquara (UNESP Araraquara), São Paulo, Brazil
[h] Department of Pharmacy, Faculty of Pharmaceutical Sciences, University of São Paulo, Prof. Lineu Prestes Avenue, 580, Bl.13, São Paulo, SP, Brazil.
[i] Department of Chemistry, University of Warwick, Coventry, CV4 7AL, UK

¥The authors contributed equally to this work
*Roberto Parise-Filho. Tel.: +55 11 30913793. E-mail: roberto.parise@usp.br

Abstract

The enzyme dihydrofolate reductase from *M. tuberculosis* (*Mt*DHFR) has a high unexploited potential to be a target for new drugs against tuberculosis (TB), due to its importance for pathogen survival. Preliminary studies have obtained fragment-like molecules with low affinity to *Mt*DHFR which can potentially become lead compounds. Taking this into account, the fragment MB872 was used as a prototype for analogue development by bioisosterism/retro-bioisosterism, which resulted in 20 new substituted 3-benzoic acid derivatives. Compounds were active against *Mt*DHFR, with IC_{50} values ranging from 7 to 40 μM, where compound **4e** not only had the best inhibitory activity (IC_{50} = 7 μM), but also was 71-fold more active than the original fragment MB872. The **4e** inhibition kinetics indicated an uncompetitive mechanism, which was supported by molecular modeling which suggested that the compounds can access an

independent backpocket from the substrate and competitive inhibitors. Thus, based on these results, substituted 3-benzoic acid derivatives have strong potential to be developed as novel *Mt*DHFR inhibitors and also anti-TB agents.

Keywords: bioisosterism, fragment optimization and drug design, *Mt*DHFR, tuberculosis.

1. Introduction

Tuberculosis (TB) is an infectious disease caused by mycobacteria, especially *Mycobacterium tuberculosis*, and generally affects the lung tissue, inducing extensive lesions [1]. WHO estimates that one-third of the world population is contaminated with *M. tuberculosis*, highlighting that about 10.4 million cases and 1.7 million deaths from TB have occurred in 2016 [2]. HIV/AIDS co-infection is an important risk factor, which increases the rate of disease progression from latent to active illness [3]. In addition, the ever-increasing number of cases of multidrug resistance to the first-choice drugs, such as rifampicin, isoniazid, ethambutol and pyrazinamide (Fig. 1A), is alarming. The phenomenon of resistance occurs, besides other factors, as a consequence of low adherence to long-term treatment [4].

Recently, *M. tuberculosis* resistant strains to bedaquiline (Fig. 1A), one of the last standing approved antituberculosis drugs, were reported [1,5,6]. The rise of new resistant strains emphasizes the urgent need for new therapeutic options against TB. The process of discovery of new therapeutics can include the validation of new potential drug targets and the search of new small molecules with antibiotic activity.

In this sense, the folate pathway is an excellent option of validated drug targets, since most of the bacteria cannot uptake folate from the medium and depend on the *de novo* biosynthesis for survival within the host [7]. The folate biosynthesis in *M. tuberculosis* is composed of six enzymes that convert GTP to tetrahydrofolate, which is essential for the production of some amino acids and DNA [8].

Dihydrofolate reductase from *Mycobacterium tuberculosis* (*Mt*DHFR) is an essential enzyme in the pathogen folate metabolism. *Mt*DHFR catalyzes the reduction of dihydrofolic acid to tetrahydrofolic acid (Fig. 1B), an essential step

for the activation of folate [9,10], using NADPH as a cofactor. Mechanistically, upon substrate binding, the nicotinamide moiety from NADPH can engage in the active site and promote catalysis. This movement of the nicotinamide moiety in and out of the active site allows the enzyme to adopt two distinct conformations, an open and a closed state, which has also been described for other DHFR's, including for human one [11].

Antifolates, such as cycloguanil, pyrimethamine, trimethoprim and WR99210 (Fig. 1C) have shown moderate inhibitory activity against *Mt*DHFR [12,13] and recent structural studies hypothesize that this is due to the enzyme flexibility, where the inhibitors would bind to only one of the two conformational states [14,15]. Nevertheless, Wiktor and colleagues demonstrated that synergism treatment using trimethoprim (Fig. 1) and sulfamethoxazole could still greatly reduce TB morbidity and mortality [16]. Although trimethoprim and other DHFR inhibitors have important roles in combating several infections, they are often not used in the clinical treatment of tuberculosis, since monotherapy has little or no effect on the *M. tuberculosis* growth [14,15].

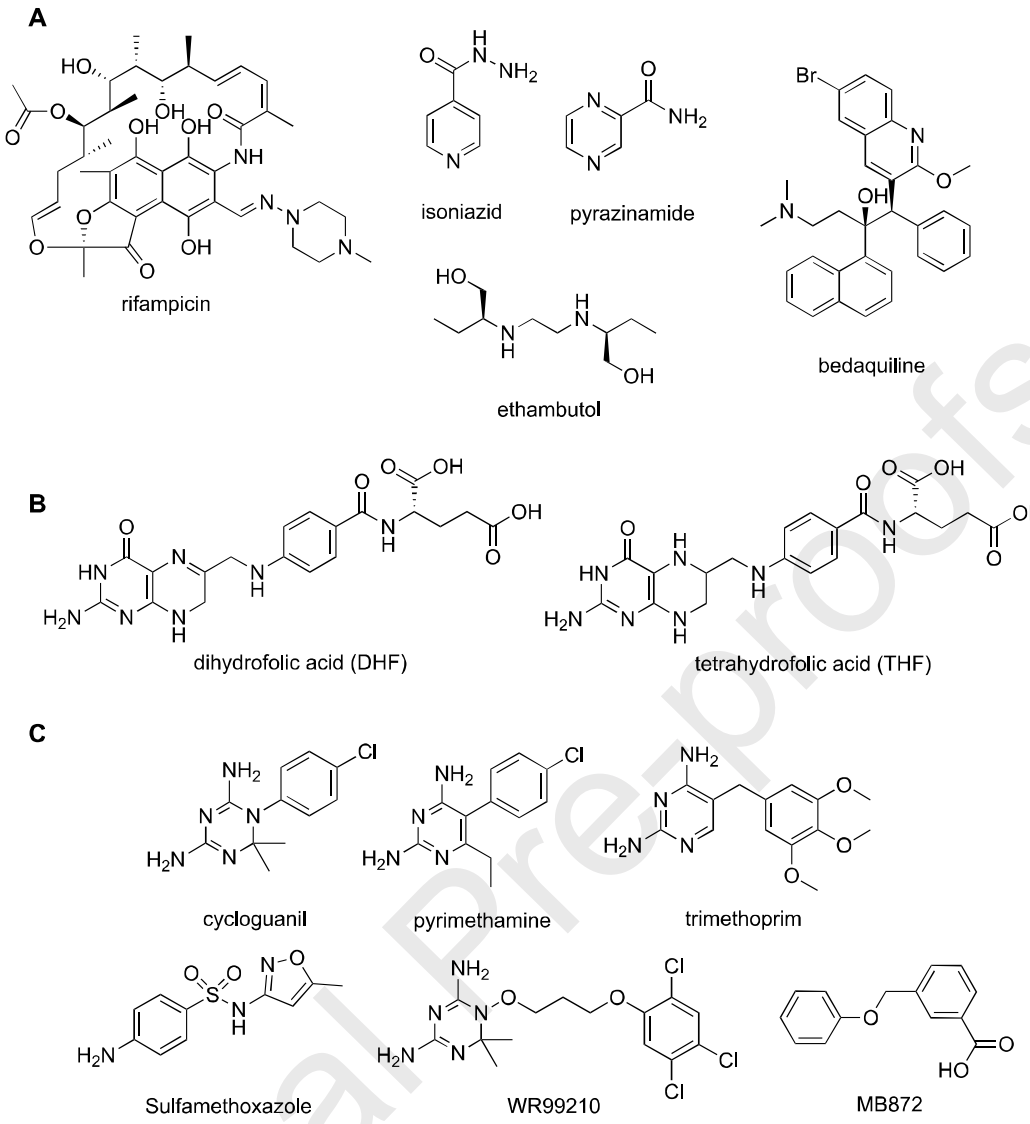

Fig. 1. A) Drugs in clinical use for tuberculosis treatment. B) The tetrahydrofolate, product from *Mt*DHFR. C) Compounds with reported activity against *Mt*DHFR.

*Mt*DHFR is an essential enzyme for the pathogen and the disruption of folate production impairs DNA synthesis and leads to metabolic stress in the mycobacteria [17–22]. However, despite the obvious druggable potential, there are still no *Mt*DHFR inhibitors available for TB treatment and, consequently, this enzyme rises as a promising drug target. Overall, DHFR inhibitors reported in the literature suffer from low selectivity against the human counterpart leading to side-effects [23], low bacteria cell permeability, and high resistance rate [14,24].

Recently, our group identified, from a fragment-based drug design campaign, the compound MB872 (Fig. 1C), which, despite a low affinity for *Mt*DHFR (0.5 mM on binding assays), has an on-target specific activity and a

moderate ligand efficiency (LE=0.26) [25]. *Mt*DHFR:NADPH in complex with MB872 suggests a potential interaction between the carboxylic acid moiety with Arg32 or Arg60, depending on the pose. So, MB872 was used as a ligand prototype for a ligand-based drug design strategy, resulting in a novel series of twenty substituted 3-benzoic acid derivatives active against *Mt*DHFR.

2. Results and Discussion

2.1. Molecular design

A screening study regarding the affinity of 1,250 chemical fragments for *Mt*DHFR identified MB872 as an interesting protein ligand with an estimated affinity value of about 0.5 mM. Later structural results [25] led us to design molecules derived from MB872. The proposed modifications address three regions (A, B and C) and a total of 20 compounds were designed and distributed into three distinct series (I, II and III), as shown in Figure 2.

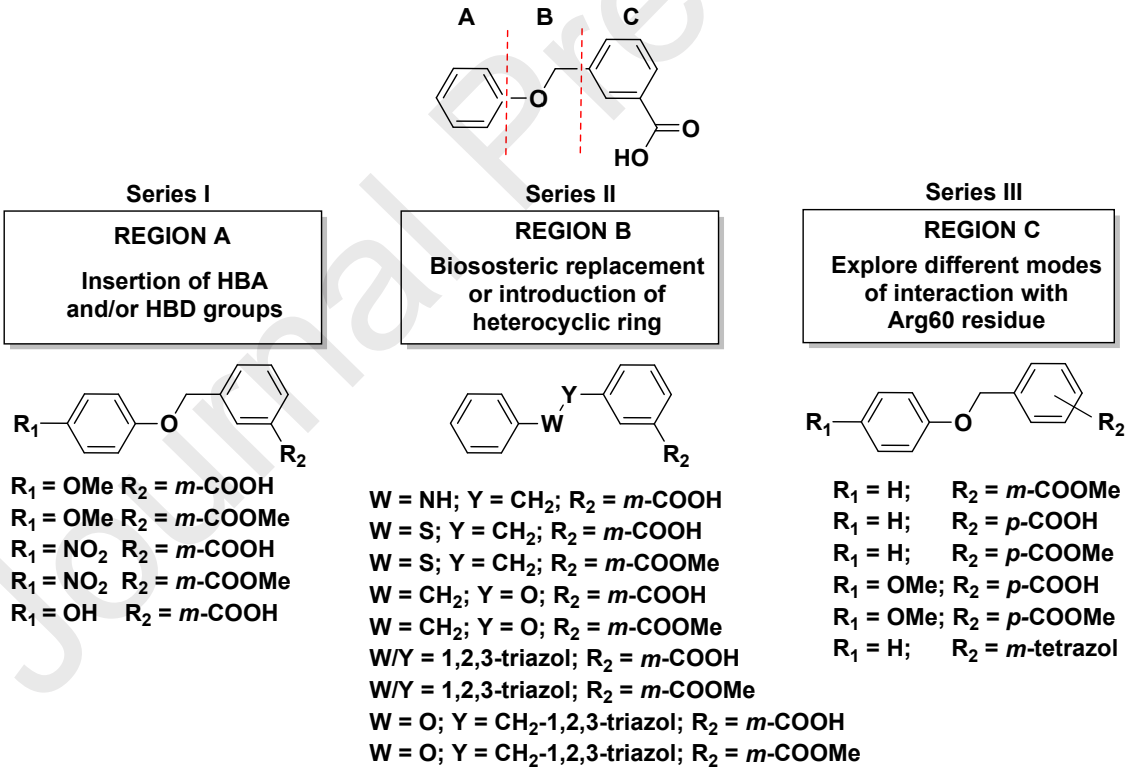

Fig. 2. Design of 20 compounds from MB872 divided into three compound series.

In 2020, Ribeiro *et al.*, reported that region A is near residues, which are potentially acceptors and donors of hydrogen bond (Tyr100, Ser49 and with the

oxygen of backbone Ile94). Thus, for the moiety A, hydrogen bonding donor and acceptor groups were introduced into the ring, which may have provided a higher possibility of polar interaction with the pocket (Fig. 2). Besides evaluating the possible hydrogen bonds, those groups might have also revealed some electronic/lipophilic effects of the substituents on the ring (*Series I*).

In region B (Fig. 2), we have employed bioisosterism and retro-bioisosterism approaches in order to obtain systematic changes of substituents and thus, generate diversities for structural and biological effects (*Series II*). Analogues containing a third ring (triazole) in the presence of a spacer group and/or a third ring in this region intended to increase hydrophobic interactions, in the case of the rings, or hydrogen bond interactions, by varying the position of the heteroatom.

In region C (Fig. 2), variations in the carboxyl group's position were performed to evaluate the relevance of ionic interaction with polar residues at the active site. Additionally, also using the bioisosterism, the carboxyl was substituted by a tetrazole, which is an acid bioisostere with a hydrophobic feature. Additionally, esters counterparts of the free carboxylic acids were synthesized to evaluate their role in the biological activity (*Series III*).

2.2. Chemistry

The prototype MB872 and the final products 4b-i, 7 and 10a-b were obtained in two/three reaction steps, as shown in Scheme 1. The synthesis of the intermediates 3a-j was based on classical alkylations of several phenols and anilines, substituted or not, with the corresponding alkyl halide. For the synthesis of compound 7, the intermediate 3j was previously reduced to the amine derivative 5, which reacted to form a diazonium salt, which underwent replacement by a cyanide ion to obtain the intermediate 6. Lastly, the nitrile underwent a 1,3-dipolar cycloaddition resulting in the tetrazole analogue 7. In order to synthesize the intermediates 9a and 9b, we also performed a 1,3-dipolar cycloaddition reaction. The compounds MB872, 4b-i and 10a-b were synthesized by hydrolysis of the methyl ester, using potassium hydroxide. Overall, we obtained 20 final products, which were characterized by melting point, ^{1}H and ^{13}C NMR.

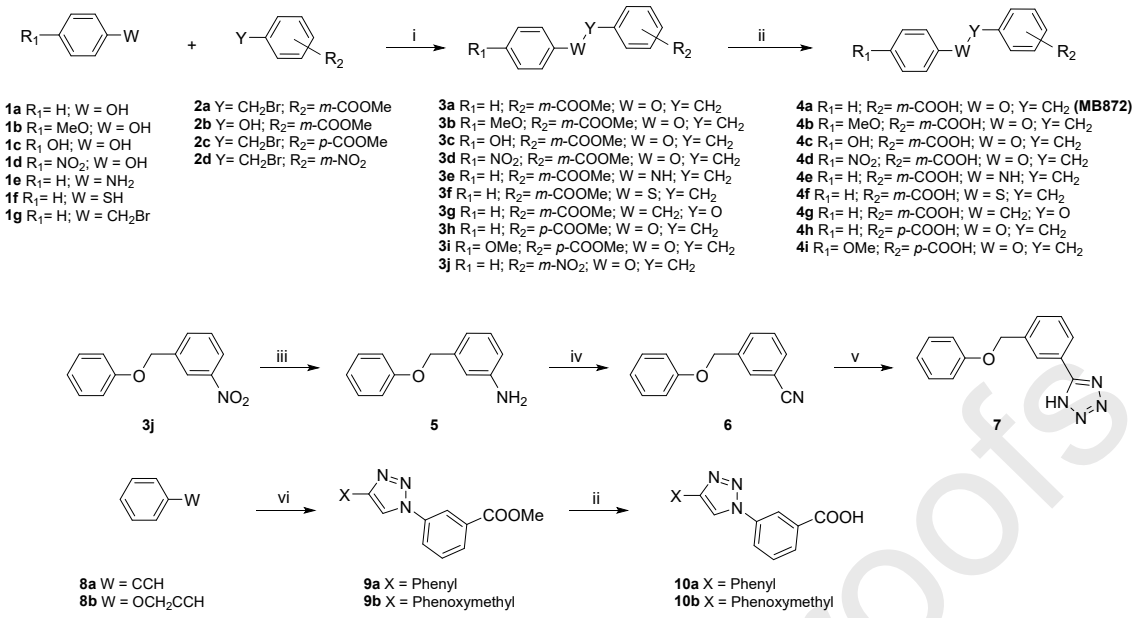

Scheme 1. Synthesis of MB872, 4b-i, 7 and 10a-b. Reagents and conditions: (i) K_2CO_3/acetone/reflux/16 h; (ii) KOH/THF/HCl/r.t./12 h; (iii) Pd/H_2/MeOH/EtOH/r.t./4 h; (iv) $NaNO_2$/HCl/CuCN/NaCN/r.t./2 h; (v) NaN_3/NH_4Cl/DMF/reflux/16 h; (vi) ascorbate/CuI/r.t./12 h/methyl 3-azidobenzoate.

2.3. Mt*DHFR inhibitory activity and structure-activity relationship (SAR)*

The *Mt*DHFR inhibitory activity of our compound series was evaluated *in vitro* by following the fluorescence emitted by *Mt*DHFR substrates when excited at 340 nm (Table 1). The enzymatic activity was measured by consuming the enzyme substrate as the product ($NADP^+$) does not emit fluorescence [27,28]. In this way, trimethoprim IC_{50} value (91 μM) was determined and used as a positive control for the assay, being in agreement with the literature data (88 μM) [15].

Most of the tested compounds were significantly more active against *Mt*DHFR (Table 1) than the initial prototype MB872 and eight of them (3d, 3f, 3i, 4c, 4d, 4e, 4i and 9b) showed stronger inhibition profile than trimethoprim. We observed that compounds from series I, which have R_1 substituents as hydroxyl in 4c (36 μM ± 0.12) and nitro group in 3d and 4d (35 μM ± 0.23 and 23 μM ± 0.12), provided increased inhibitory activities ranging from 13- to 21-fold, respectively, when compared to MB872 (>500 μM). Moreover, 4d (-NO_2) had the inhibitory activity increased by about 1.5-fold in comparison to 4c (-OH), which might have been caused by electron density decrease of the aromatic ring, due to the resonance withdrawing effect of the nitro group. Regarding the introduction of methoxyl in R_1, an electron donor group (derivatives 3b and 4b presented IC_{50} of 242 μM ± 0.08 and 119 μM ± 4.8, respectively), the compounds did not show

a significant inhibitory activity when compared to MB872 (>500 μM), although they were modestly active.

Compound 4e (Series II), a classical bioisostere of MB872, was the most active against *in vitro Mt*DHFR (IC_{50} values of 7 ± 0.13 μM) and exhibited better activity than the original prototype (by approx. 71-fold) and trimethoprim (by 13-fold). The bioisostere replacement, exchanging the oxygen atom by nitrogen, provided an extra hydrogen-bond donor feature, which could allow additional stabilizing interactions. Compounds with a free ionizable carboxylic acid group in R_2 were active (4c, 4d, and 4i had an IC_{50} of 36 μM, 23 μM, and 31 μM, respectively), in comparison to esterified versions 3f and 9b, which were less active (76 μM ± 0.01 and 81 μM ± 0.11, respectively), or even inactive (3g and 9a). Noteworthy, the insertion of a triazole group in region B led to a complete loss of inhibitory effect (9a and 10a). Moreover, the insertion of the OCH_2-1,2,3-triazole group (9b and 10b) was also not beneficial to *Mt*DHFR inhibitory activity.

Compounds from series III, containing a methoxyl group in R_1 and associated with the *para*-substitution in R_2, had a significant increase in the enzyme inhibition, as observed for compounds 3i and 4i (26 μM ± 0.16 and 31 μM ± 0.10), which are some of the most active derivatives of series III. Therefore, analogues 3i and 4i presented IC_{50} values 16- and 19-fold lower than the prototype MB872, respectively. Finally, in series III, the bioisostere group tetrazole in *meta*-substitution (compound 7) was not beneficial, demonstrating low activity against *Mt*DHFR (IC_{50} = 454 μM).

Table 1. *Mt*DHFR inhibition activity.

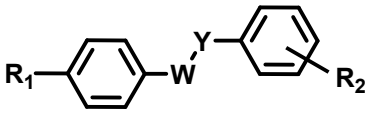

Compound	R_1	W	Y	R_2	IC_{50} (μM) ± SD[a]	LLE
MB872	H	O	CH_2	*m*-COOH	>500	0.98
TMP[b]					91 ± 0.16	2.59
3a	H	O	CH_2	*m*-COOMe	>500	0.05
3b	OMe	O	CH_2	*m*-COOMe	242 ±0.08	1.31
3d	NO_2	O	CH_2	*m*-COOMe	35 ±0.23	2.24
3f	H	S	CH_2	*m*-COOMe	76 ±0.01	1.24

3g	H	CH_2	O	*m*-COOMe	>500	0.98
3h	H	O	CH_2	*p*-COOMe	152 ±0.10	0.56
3i	OMe	O	CH_2	*p*-COOMe	26 ±0.16	1.35
4b	OMe	O	CH_2	*m*-COOH	119 ±4.8	1.62
4c	OH	O	CH_2	*m*-COOH	36 ±0.12	2.40
4d	NO_2	O	CH_2	*m*-COOH	23 ±0.13	2.42
4e	H	NH	CH_2	*m*-COOH	7 ±0.13	3.10
4f	H	S	CH_2	*m*-COOH	128 ±0.11	1.01
4g	H	CH_2	O	*m*-COOH	230 ±0.09	1.31
4h	H	O	CH_2	*p*-COOH	442 ±0.13	1.03
4i	Ome	O	CH_2	*p*-COOH	31 ±0.1	2.20
7	H	O	CH_2	*m*-tetrazole	454 ±0.15	0.176
9a	H	1,2,3-triazole		*m*-COOMe	ND[c]	
9b	OMe	1,2,3-triazole		*m*-COOMe	81 ±0.11	0.89
10a	H	1,2,3-triazole		*m*-COOH	ND	
10b	OMe	1,2,3-triazole		*m*-COOH	>500	Approx. 1.04

[a]Data are expressed as means and the standard deviation intervals (SD) were obtained from three independent experiments. [b]TMP stands for trimethoprim. [c]ND stands for not determined. LLE stands for ligand lipophilicity efficiency, which is calculated from the difference between pIC_{50} values and the LogP.

The most potent compound (4e) against *Mt*DHFR was selected for further enzyme kinetics studies. The Michaelis constant (K_m) and the maximum velocity (V_{max}) were determined, in the presence of varying concentrations of inhibitor. The substrate's K_m remained constant (0.22 μM ± 0.04), while V_{max} varied (0.34, 0.41 and 0.43), when tested using increasing concentrations of compound 4e, which is consistent with uncompetitive inhibition [29,30]. The results suggest that the binding mode explores a distinct (sub-)pocket from the substrate or cofactor binding sites. Srinivasan and colleagues [31] reported ten novel small-molecule inhibitors of *E. coli* DHFR (*Ec*DHFR), which have shown a unique uncompetitive inhibition mechanism, acting by displacing the DHF substrate. However, the precise structural binding mode suggested based on pocket similarity analyses, would need further validation.

2.4. Uncompetitive DHFR inhibition as a result of compounds accessing a unique backpocket

In order to understand at the molecular level the uncompetitive mechanism of the most potent designed inhibitor (4e), comparative molecular dynamics (MD) simulation of co-crystallized substrate (DHF) and known competitive DHFR inhibitors (methotrexate – MTX, pemetrexed – PMX and diaverdine – DIA), as well as docking poses of selected compounds from our series (namely, 4b, 4e and 4h) were performed. Compound 4e was chosen as the most potent of the series, 4b due to the change in the linker region and 4h aiming to discuss the different positioning of the R_2 substituent.

*Mt*DHFR can shift between two conformations, from the perspective of the loop covering the active site: one open, where it can receive the substrates and the cofactor, and another closed, which is bound to the cofactor. Simulations of the *Mt*DHFR closed conformation in complex with DHF revealed stable hydrogen interactions between the DHF pteridine ring N8 and the Ile5 backbone's oxygen atom (Fig. 3A) and between the carboxylic acid moiety and the Arg32 and Arg60 sidechains (Fig. 3A,B). The original crystal structures of *Mt*DHFR complexed with DHF and MTX showed that the pteridine rings have different conformations [26]. The different initial conformations reflect on different stable interactions of the pteridine moiety, such as the MTX 2,4-diamino group addressing Ile5 and Ile94 (Fig. 3A,C) oxygen backbone atoms, while the DHF 4-oxopteridine group points away from them (Fig. 3A,B). Interestingly, even though PMX does not directly interact with Ile94 main chain, we observed an intermittent water-mediated hydrogen bond with N7 from the pyrrolopyrimidine ring (40% of the simulation time, data not shown). The orientation of the dihydropyrimidine ring is further stabilized by the hydrogen bond interaction between the sidechain Asp27 (Fig. 3A for frequency) and the 2,4-diamino moieties of the MTX and DIA inhibitors (Fig. 3C and E, respectively) and by the 2-amino pyrrolopyrimidine of the PMX (Fig. 3D). On the other hand, the stabilization due to the Asp27 interaction, thus occupation of this particular pocket, cannot be observed in our series (Fig. 3A and Fig. 4).

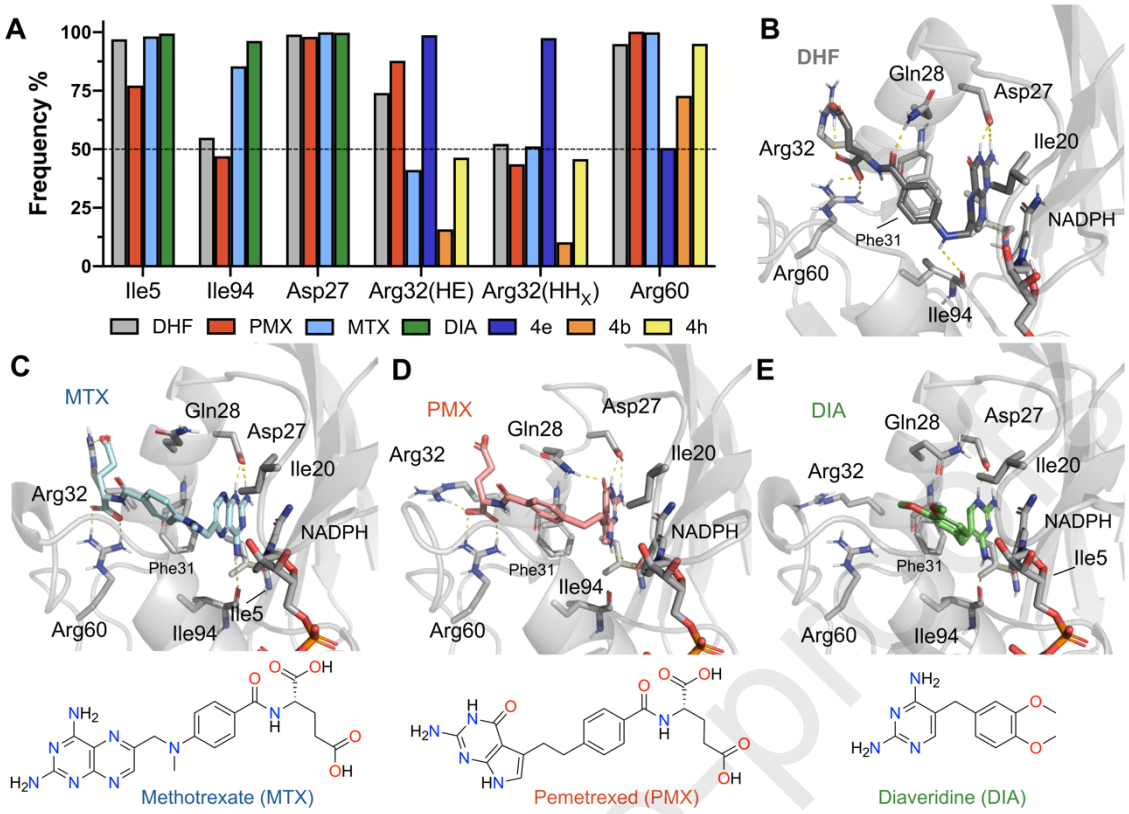

Fig. 3. A) Frequency of hydrogen interactions observed along with the production phase of molecular dynamics simulation. Arginine 32's hydrogen bond interactions were separated into two groups: HE, performed by the hydrogen's NH in the base of the guanidinium group, and HHx which is one of either HH atoms in the extremity of this group, indistinguishably. Representative snapshots from the molecular dynamics simulation (1 µs per system), highlighting the residues involved in interactions B) DHF (PDB ID: 6NND), C) MTX (1DF7), D) PMX (6NNC) and E) DIA (6NNE). Interactions are represented by dashed lines. DHFR residues are colored according to the atom types of the interacting amino acid residues (protein's carbon, light gray; nitrogen, blue; oxygen, red).

All known DHFR inhibitors, except DIA (Fig. 3E), share a common hydrogen bond and ionic interaction networks between their carboxylic acid moieties and the Arg32 and Arg60 (Fig. 3A – D). A similar network is also explored by our inhibitors (Fig.3A and Fig. 4), independently from the ring attachment point (*-meta* or *-para*), as long as the substituent remains unesterified and, therefore, ionizable. Moreover, hydrophobic (Supplementary Data, Fig. 4A) and π-π interactions (Supplementary Data, Fig. 4B) were suggested by the initial docking pose with our inhibitors and also between the Phe31 and pteridine/pyrrolopyrimidine moieties from known inhibitors, which were not maintained during the simulations.

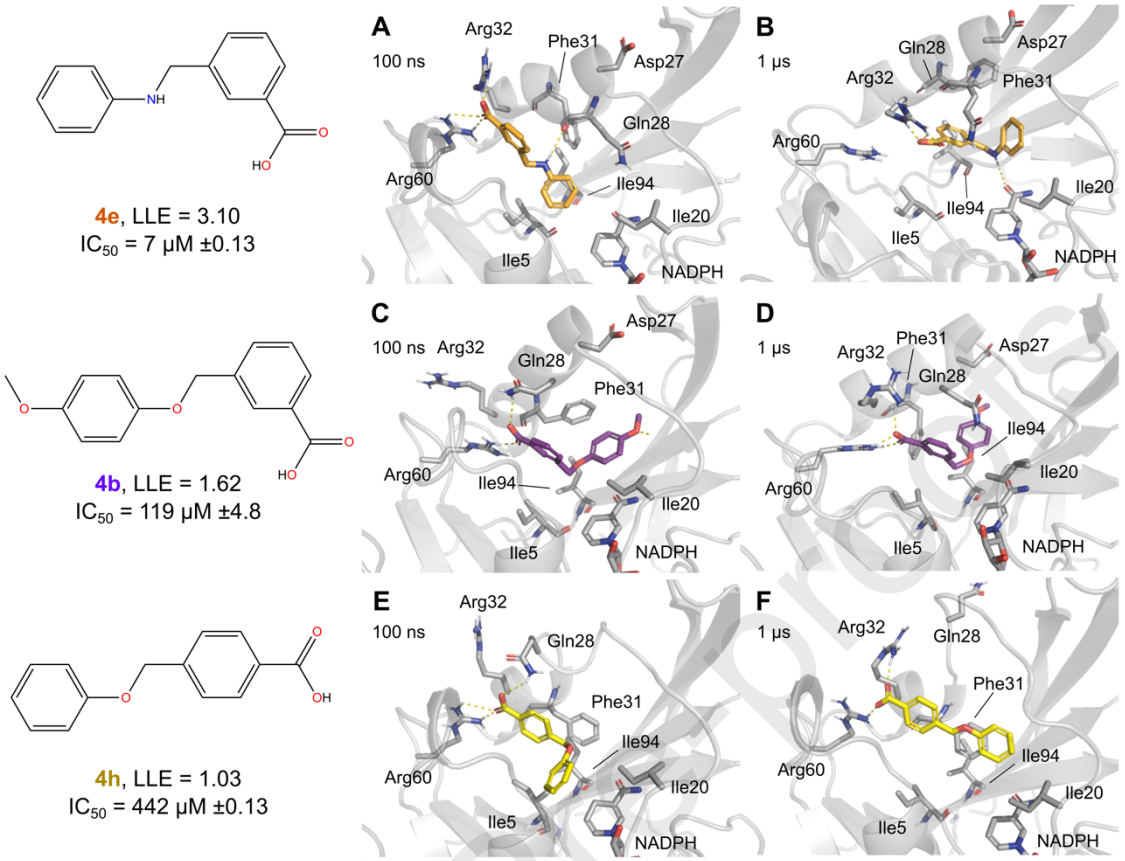

Fig. 4. Representative snapshots from the molecular dynamics simulation, highlighting the residues involved in interactions: compound 4e (A – 100 ns, B – 1 μs), compound 4b (C, D) and compound 4h (E, F). DHFR residues are colored according to the atom types of the interacting amino acid residues (protein's carbon, light gray; nitrogen, blue; oxygen, red).

The most active inhibitor from the series (4e, Fig. 4A,B) establishes transient interactions with the Gln28, Ile20 and Ile94 main-chain oxygen atoms. However, the proposed binding mode for 4e cannot be explained by a single conformation, as highlighted by the different positioning of the phenoxy ring upon simulation, seldomly interacting with Phe31. Interestingly, simulations with the least potent inhibitors (4b and 4h) show the inability to stabilize the loop covering the active site, even after 1 μs simulation (Fig. 4D,F). We hypothesize that compounds with an uncompetitive inhibition mechanism would address only one of the two possible DHFR conformations (open and closed) with the most potent ones stabilizing the closed state. However, we do not discard the possibility of the compounds to address other transient pockets or have an effect on higher quarternary structures [11,32]. Finally, compound 4e presented the highest LLE

values among the tested set, including controls. This suggests that, despite the low potency, compound 4e has the potential to be further optimized into a great lead compound.

Interestingly, the *Ec*DHFR inhibitors SAR model describes the presence of two benzene rings, a spacer with a minimum of three degrees of freedom and the presence of polar substituents, which are able to perform hydrogen bond interactions, on the benzene rings [31]. Those chemical features are shared both by our *Mt*DHFR inhibitors and also by stilbenoid, deoxybenzoin and chalcone scaffolds, with a reported uncompetitive mechanism of action [31]. Moreover, in the described uncompetitive inhibition [31], the inhibitor reversibly binds to the ES_1 complex (DHFR + NADPH) yielding an inactive ES_1I complex. Hence, V_{max} in the presence of the inhibitor would be lower than in its absence, without affecting the K_m, which we also observe in the 4e inhibition (Supplementary Data, Fig. 1 and Table 1).

We therefore suggest that 4e could also present an uncompetitive inhibition mechanism since our inhibitors do not share the most essential interaction features with known substrate competitive DHFR inhibitors (for instance, the interaction with Asp27 and Ile94), but rather occupy a unique pocket near the loop, composed by Arg32, Arg60 and, intermittently, interacts with Phe31.

3. Conclusions

Novel substituted 3-benzoic acid derivatives were designed and synthesized as potential inhibitors against *Mt*DHFR. After having their activities evaluated, compound 4e showed the best inhibitory activity with an IC_{50} of 7 μM, which is 71-fold more active than the start fragment prototype MB872. Moreover, the kinetics of *Mt*DHFR inhibition revealed that 4e did not compete with DHF or NADPH to inhibit *Mt*DHFR since K_m keeps constant, while V_{max} changed considerably, indicating an uncompetitive mechanism. Hence, 4e is the first uncompetitive inhibitor reported for DHFR from *M. tuberculosis*, with a suggested binding mode that partially accesses the binding pocket of known inhibitors, in the active site. In conclusion, these findings provide new insights into substituted 3-benzoic acids and 4e analogs can have strong potential for further development into new promising anti-TB compounds.

4. Experimental section

4.1 *Mt*DHFR *production*

DHFR from *Mycobacterium tuberculosis* was purified according to the protocol described in Ribeiro *et al*. (2019) [26]. Briefly, a pET28(a)$^{+}$ vector carrying the *folA* gene was transformed in BL21(DE3) competent cells. The transformed cells were grown at a temperature of 37 °C until the OD600 reached 0.6, when the protein expression was induced by the IPTG (0.2 mM) at 18 ºC during 18 h. After that, cells were harvested by centrifugation and resuspended in a buffer containing 20 mM $NaPO_4$ and 50 mM KCl (Buffer A). Cells were disrupted using a sonicator (Branson Sonifier) in presence of 1 mM PMSF, 0.2 mg.mL^{-1} lysozyme and 1 mM DNAse (Sigma–Aldrich) and cell lysate was clarified by centrigutaion at 13,000 g (at 4 °C for 1 h). The purification was performed using an IMAC column charged with Ni^{2+} and an imidazole gradient in an Äkta Purifier System using a Buffer B (Buffer A in addition to increasing concentrations of imidazole, until 500 mM) and by gel filtration using a S200 chromatography column. The pure protein was eluted using Buffer A, concentrated up to 10 mg/mL and stored at -80 °C until use.

4.1.1 Kinetics assay

Kinetics measurements were carried out Fluorimeter (TECAN Infinite Pro M200) using a standard assay by Meek and coworkers [33], at pH 7.5 (50 mM sodium phosphate). The Michaelis-Menten constant was calculated for the NADPH cofactor and DHF substrate by following a decrease in fluorescence at 480 nm, upon excitation at 340 nm, using a range of concentrations (0.1 to 100 µM).

For IC_{50} determination and mode of inhibition studies, we used a classic kinetic assay. Therefore, the IC_{50} determination was carried out in balanced conditions (0.09 µM *Mt*DHFR, 5 µM DHF and 10 µM cofactor NADPH) at pH 7.5 (50 mM sodium phosphate buffer) by investigating the effect of, at least, six concentrations (0.01 to 30 µM) of each compound over the catalytic activity of *Mt*DHFR. All compounds were solubilized in DMSO (at the maximum concentration of 5% during the assays). The inhibition percentage was calculated with reaction velocities (Inhibition %=(100-V_1/V_c)x100)), where V_1 represents the initial velocity in the presence of the putative *Mt*DHFR inhibitor and V_c is the initial

velocity of the control (5% DMSO v/v). The IC_{50} values were calculated using least-squares non-linear regression, available in the GraphPad Prism (GraphPad® software, version 8.1, La Jolla, California, USA). The mechanism using the same reaction conditions as above with the most potent derivative (4e) was investigated by determining its effect over the apparent K_m and V_{max} values for DHF and NADPH. Apparent K_m and V_{max} values in the presence of the inhibitor were obtained by non-linear regression to the Michaelis-Menten equation and compared to each other (F test of the sim of the extra squares, values considered significantly different when $p < 0.05$), as available in the GraphPad Prism (GraphPad® software, version 8.1, GraphPad software, version 8.1, La Jolla, California, USA, www.graphpad.com).

4.2 Chemistry

All reagents were purchased from Synth, Merck and Sigma Aldrich and were used directly without any purification. Thin-layer chromatography (TLC) was performed using silica GF_{254} gel-coated aluminum plates with a fluorescent indicator (Merck). The TLCs were revealed by UV light irradiation at 254 nm and/or staining solution. Chromatographic purification was performed on silica gel columns (SiGel 60, 220 – 440 mesh, Sigma-Aldrich). The purity of the synthesized compounds was assessed on a Shimadzu Prominence HPLC system using a C_{18} column (5 µm, 150 x 4.6 mm, Gemini), with ultraviolet detection set at 254 nm. The mobile phase employed was deionized water (Solvent A) and acetonitrile containing 0.1% trifluoroacetic acid (Solvent B) in gradient elution. The overall run time was 20 minutes and the injection volume was 20 µL. For structural characterization, ^{1}H NMR and ^{13}C NMR spectra were recorded on a Bruker Advanced DPX-300 NMR spectrometer (300 MHz and 75 MHz, respectively) and the samples were prepared in $CDCl_3$, CD_3OD, D_2O or DMSO-d_6. Chemical shifts are given in parts per million (ppm), with tetramethylsilane as an internal standard. The following multiplicity abbreviations are used: singlet (s), doublet (d), broad singlet (br s), triplet (t) and multiplet (m). Coupling constants (J values) are given in Hertz (Hz). All NMR spectra for each compound can be found in the Supplementary Data.

4.2.1 Procedure for the synthesis of compounds 3a-i

Methyl 4-(bromomethyl)benzoate or methyl 3-(bromomethyl)benzoate (1 mmol) was dissolved in acetone (5 mL/mmol) and then potassium carbonate (3 eq., 3 mmol) was added. The compound to be alkylated (1a-g) (1.2 eq.) was added to the mixture and the reaction was kept under reflux for 16 h. The solvent was then removed under reduced pressure. The residue was solubilized in ethyl acetate and then washed with deionized water (3 x 10 mL). The organic layer was dried (Mg_2SO_4), filtered, and concentrated under reduced pressure. The products were purified by flash column chromatography (EtOAc/hexane in the proportion of 7:3) [34].

Methyl 3-phenoxymethyl benzoate (3a)

Yellow liquid; yield: 74%. ^{1}H NMR (300 MHz, $CDCl_3$) δ (ppm): 8.11 (s, 1H, H2), 8.00 (d, *J* = 7.7 Hz, 1H, H6), 7.64 (d, *J* = 7.7 Hz, 1H, H4), 7.45 (t, *J* = 7.7 Hz, 1H, H5), 7.29 (t, *J* = 8.0 Hz, 2H, H5'-H3'), 6.98 (m, 3H, H2'-H4'-H6') 5.10 (s, 2H, H7), 3.92 (s, 3H, H9). ^{13}C NMR (75 MHz, $CDCl_3$) δ (ppm): 166.9 (C8), 158.6 (C1'), 137.6 (C3), 131.8 (C4), 130.5 (C6), 129.5 (C5'-C3'), 129.1 (C1), 128.7 (C2), 128.5 (C5),121.2 (C4'), 114.9 (C6'-C2'), 69.4 (C7), 52.1 (C9).

Methyl 3-((4-methoxyphenoxy)methyl)benzoate (3b)

White solid; yield: 70%. ^{1}H NMR (300 MHz, $CDCl_3$) δ (ppm): 8.09 (s,1H, H2), 7.99 (d, *J* = 7.6 Hz, 1H, H6), 7.62 (d, *J* = 7.3 Hz, 1H, H4), 7.44 (t, *J* = 7.6 Hz, 1H, H5), 6.90 (d, *J* = 8.6 Hz, 2H, H5'-H3') 6.83 (d, *J* = 8.9 Hz, 2H, H6'-H2'), 5.04 (s, 2H, H7), 3.92 (s, 3H, H9), 3.76 (s, 3H, H10). ^{13}C NMR (75 MHz, $CDCl_3$) δ (ppm): 166.9 (C8), 154.2 (C4'), 152.7 (C1'), 137.8 (C3), 131.8 (C4), 130.5 (C6), 129.1 (C1), 128.6 (C2),128.5 (C5), 115.9 (C6'-C2'), 114.7 (C5'-C3'), 70.2 (C7), 55.7 (C10), 52.1 (C9).

*Methyl 3-((4-nitrophenoxy)methyl)benzoate (*3d*)*

Yellow solid; yield: 74%. ^{1}H NMR (300 MHz, $CDCl_3$) δ (ppm): 8.21 (d, *J* = 9.1 Hz, 2H, H5'-H3'), 8.11 (s, 1H, H2), 8.04 (d, *J* = 7.7 Hz, 1H, H6), 7.63 (d, *J* = 7.5 Hz, 1H, H4), 7.49 (t, *J* = 7.7 Hz, 1H, H5) 7.04 (d, *J* = 9.1 Hz, 2H, H6'-H2'), 5.20 (s, 2H, H7), 3.94 (s, 3H, H9). ^{13}C NMR (75 MHz, $CDCl_3$) δ (ppm): 166.6 (C8), 163.4 (C1'), 141.9 (C4'), 136.0 (C3), 131.8 (C1), 130.8 (C4), 129.6 (C6), 128.9 (C2), 128.3 (C5), 128.6 (C5') 126.0 (C3'), 114.9 (C6'-C2'), 70.1 (C7), 52.2 (C9).

3-((Phenylthio)methyl)benzoate (3f)

Yellow liquid; yield: 77%. ^{1}H NMR (300 MHz, ($CDCl_3$): δ = 7.96 (s, 1H, H2), 7.90 (d, *J* = 7.7 Hz, 1H, H6), 7.45 (d, *J* = 7.6 Hz, 1H, H4), 7.38 – 7.14 (m, 5H), 4.13 (s, 2H, H7) 3.89 (s, 3H, H9). ^{13}C NMR (75 MHz, $CDCl_3$) δ (ppm): 166.8 (C8), 138.1 (C1'), 135.7 (C3), 133.3 (C4), 130.4 (C6), 130.3 (C3'-C5'), 130.0 (C1), 128.9 (C2), 128.5 (C5), 128.8 (C4'), 126.7 (C6'-C2'), 52.1 (C9), 38.9 (C7).

Methyl 3-(benzyloxy)benzoate (3g)

White solid; yield: 73%. ^{1}H NMR (300 MHz, $CDCl_3$) δ (ppm): 7.66 (s, 1H, H2), 7.64 (d, *J* = 6.7 Hz, 1H, H6), 7.47 – 7.29 (m, 6H), 7.19 – 7.14 (m, 2H), 5.10 (s, 2H, H7), 3.91 (s, 3H, H9). ^{13}C NMR (75 MHz, $CDCl_3$) δ (ppm): 166.9 (C8), 158.8 (C3), 136.6 (C1'), 131.5 (C1), 129.4 (C5), 128.6 (C5'-C3'), 128.1 (C1), 127.5 (C6'-C2'), 122.3 (C4), 120.3 (C6), 115.2 (C2), 70.2 (C7), 52.1 (C9).

*Methyl 4-(benzyloxy)benzoate (*3h*)*

Brown solid; yield: 92%. ^{1}H NMR (300 MHz, $CDCl_3$) δ (ppm): 8.05 (d, *J* = 8.2 Hz, 2H, H6-H2), 7.50 (d, *J* = 8.0 Hz, 2H, H5-H3), 7.29 (t, *J* = 6.0 Hz, 2H, H5'-H3'), 6.95-6.99 (m, 3H, H6'-H2'-H4'), 5.13 (s, 2H, H7), 3.92 (s, 3H, H9). ^{13}C NMR (75 MHz, $CDCl_3$) δ (ppm): 166.9 (C8), 158.5 (C1'), 142.4 (C4), 129.9 (C6-C2), 129.6 (C5-C3), 127.0 (C5'-C3'), 121.3 (C4'), 114.9 (C6'-C2'), 69.3 (C7), 52.1 (C9).

*Methyl 4-((4-methoxyphenoxy)methyl)benzoate (*3i*)*

Brown solid; yield: 84%. ^{1}H NMR (300 MHz, $CDCl_3$) δ (ppm): 8.04 (d, *J* = 8.2 Hz, 2H, H6-H2), 7.49 (d, *J* = 8.2 Hz, 2H, H5-H3), 6.90 (d, *J* = 9.2 Hz, 2H, H5'-H3'), 6.83 (d, *J* = 9.2 Hz, 2H, H6'-H2'), 5.08 (s, 2H, H7), 3.92 (s, 3H, H9), 3.76 (s, 3H, H10). ^{13}C NMR (75 MHz, $CDCl_3$) δ (ppm): 166.9 (C8), 154.2 (C4'), 152.7 (C1'), 142.6 (C4), 129.8 (C5-C3), 127.0 (C6-C2), 115.9 (C6'-C2'), 114.7 (C5'-C3'), 70.1 (C7), 55.7 (C10), 52.1 (C9).

4.2.2 Synthesis of triazoles

4.2.2.1 Synthesis of reagent methyl 3-aminobenzoate

Methyl 3-amino benzoate was dissolved in water, then the medium was acidified (at 0 °C) using 5% of HCl solution. Afterward, a solution of $NaNO_2$

(2.5 eq) was added dropwise and the mixture was kept under stirring. After 30 min, NaN_3 (1.6 eq.) was added slowly. At the end of the bubbles, the mixture reaction was extracted with EtOAc. The organic layer was dried over with Na_2SO_4, filtered, and concentrated under reduced pressure [35].

Methyl 3-aminobenzoate

Colorless liquid; yield: 95%. ^{1}H NMR (300 MHz, $CDCl_3$) δ (ppm): 7.85 – 7.76 (m, 1H, H6), 7.74 – 7.61 (m, 1H, H2), 7.42 (t, *J* = 7.9 Hz, 1H, H5), 7.21 – 7.18 (m, 1H, H4), 3.93 (s, 3H, H8). ^{13}C NMR (75 MHz, $CDCl_3$) δ (ppm): 166.2 (C7), 140.6 (C3), 131.9 (C5), 129.8 (C1), 126.0 (C4), 123.4 (C6), 120.0 (C2), 52.3 (C8).

4.2.2.2 Synthesis of reagent (prop-2-yn-1-yloxy)benzene

Propargyl bromide (80% in toluene) (1 mmol) was dissolved in acetone (5 mL/mmol) and then K_2CO_3 (3 eq, 3 mmol) was added. Phenol (1.2 eq.) was added under stirring and the reaction was maintained at reflux for 16 hours. In the end, the solvent was removed under reduced pressure and the mixture was solubilized in EtOAc and then it was washed with deionized water (3 x 10 mL). The organic layer was dried (Na_2SO_4), filtered, and concentrated in vacuum. The residue was purified by flash column chromatography (EtOAc/hexane) [34].

(prop-2-yn-1-yloxy) benzene

Yellow liquid; yield: 91%. ^{1}H NMR (300 MHz, $CDCl_3$) δ (ppm): 7.33 – 7.27 (m, 2H, H3-H6), 7.01 – 7.61 (m, 3H, H2-H5-H4), 4.68 (d, *J* = 2.4 Hz, 2H, H7), 2.50 (t, *J* = 2.4 Hz, 1H, H9) . ^{13}C ^{1}H NMR (75 MHz, $CDCl_3$) δ (ppm): 157.6 (C1), 129.5 (C3-C6), 121.6 (C4), 114.9 (C2-C5), 78.7 (C8), 75.4 (C9), 55.8 (C7).

4.2.2.3 Cycloaddition – Synthesis of compounds 9a-b

In the mixture of tetrahydrofuran/H_2O or *t*-BuOH/H_2O were added CuI (1.1 eq.) and sodium ascorbate (0.5 eq.). The reaction was kept under stirring and light protection for 12 hours. The mixture was filtered through Celite® 545, then the solvent was evaporated under reduced pressure and the residue was dissolved in ethyl acetate and washed with and water (1:1). Finally, the products were purified using flash chromatography column (EtOAc/hexane) to give the compounds 9a-b [36].

*Methyl 3-(4-phenyl-1*H*-1,2,3-triazol-1-yl)benzoate (*9a*)*

Yellow solid; yield: 30%. ^{1}H NMR (300 MHz, $CDCl_3$) δ (ppm): 8.40 (s, 1H, H8), 8.27 (s, 1H, H2), 8.12 (d, *J* = 6.8 Hz, 1H, H6), 8.09 (d, *J* = 7.0 Hz, 1H, H4), 7.91 (d, *J* = 7.1 Hz, 2H, H6'-H3'), 7.63 (t, *J* = 7.9 Hz, 1H, H5) 7.46 (t, *J* = 7.3 Hz, 2H, H5'-H3'), 7.37 (t, *J* = 7.3 Hz, 1H, H4') 3.98 (s, 3H, H9). ^{13}C NMR (75 MHz, $CDCl_3$) δ (ppm): 165.8 (C9), 148.7 (C7), 137.2 (C3), 131.9 (C1), 130.1 (C1'), 129.6 (C5), 128.9 (C3'-C5'), 128.6 (C4'), 125.9 (C2'-C6'),124.7 (C4), 121.0 (C8), 117.5 (C2), 52.6 (C10).

*Methyl 3-(4-(phenoxymethyl)-1*H*-1,2,3-triazol-1-yl)benzoate (*9b*)*

Yellow solid; yield: 80%. ^{1}H NMR (300 MHz, $CDCl_3$) δ (ppm): 8.35 (s, 1H, H9), 8.13 – 8.10 (m, 2H, H2-H6), 8.02 (d, *J* = 8.1 Hz, 1H, H4), 8.09 (d, *J* = 7.0 Hz, 1H, H4), 7.61 (t, *J* = 8.0 Hz, 1H, H5), 7.31 (t, *J* = 7.9 Hz, 2H, H5'-H3'), 7.04 – 6.96 (m, 3H, H6'-H2'-H4'), 5.31 (s, 2H, H7), 3.96 (s, 3H, H11). ^{13}C NMR (75 MHz, $CDCl_3$) δ (ppm): 165.7 (C10), 158.2 (C1), 145.4 (C8), 137.2 (C3), 132.0 (C1), 130.0 (C5), 129.6 (C3'-C5'), 129.7 (C6) 124.8 (C4), 121.4 (C2), 121.2 (C4'), 120.8 (C9), 114.8 (C2'-C6'), 62.0 (C7), 52.5 (C11).

4.2.2.4 Hydrolysis of esters – Synthesis of compounds MB872, 4b-l and 10a-b

Methyl esters (1 eq, 1 mmol) were dissolved in THF and water (2 mL/mmol), after a KOH solution 2 mol/L was added (3 eq, 3 mmol, 1.5 mL solution). The mixture was kept under stirring and room temperature until TLC indicated that no starting material remained. THF was removed under reduced pressure and the mixture was acidified with a solution of HCl (5% v/v) until pH 2.0. The precipitate was filtered and collected. Lastly, the products were purified by flash chromatography column using DCM/MeOH (9:1, respectively), as the eluent system [34].

*3-Phenoxymethyl benzoic acid (*MB872*)*

White solid; yield: 84%. ^{1}H NMR (300 MHz, DMSO-d_6) δ (ppm): 8.04 (s, 1H, H2), 7.92 (d, *J* = 7.7 Hz, 1H, H6), 7.70 (d, *J* = 7.6 Hz, 1H, H4), 7.53 (t, *J* = 7.7 Hz, 1H, H5), 7.31 (t, *J* = 7.9 Hz, 2H, H5'-H3'), 7.03 (d, *J* = 8.0 Hz, 2H, H2'-H6') 6.95 (t, *J* = 7.3 Hz, 1H, H4'), 5.18 (s, 2H, H7). ^{13}C NMR (75 MHz, DMSO-d_6) δ (ppm): 167.1

(C8), 158.2 (C1'), 137.7 (C3), 131.8 (C1), 131.0 (C4), 129.4 (C5'-C3'), 128.7 (C6), 128.6 (C2), 128.2 (C5), 120.8 (C4'), 114.8 (C6'-C2'), 68.5 (C7).

*3-((4-Methoxyphenoxy)methyl)benzoic acid (*4b*)*

White solid; yield: 77%. ^{1}H NMR (300 MHz, DMSO-d_6) δ (ppm): 8.02 (s, 1H, H2), 7.90 (d, *J* = 7.7 Hz, 1H, H6), 7.67 (d, *J* = 7.6 Hz, 1H, H4), 7.51 (t, *J* = 7.6 Hz, 1H, H5), 6.96 (d, *J* = 9.1 Hz, 2H, H5'-H3'), 6.86 (d, *J* = 9.1 Hz, 2H, H6'-H2'), 5.12 (s, 2H, H7), 3.69 (s, 3H, H10). ^{13}C NMR (75 MHz, DMSO-d_6) δ (ppm): 167.2 (C8), 153.6 (C4'), 152.1 (C1'), 137.9 (C3), 131.7 (C1), 131.0 (C4), 128.6 (C6), 128.5 (C2), 128.1 (C5), 115.8 (C6'-C2'), 114.6 (C5'-C3'), 69.1 (C7), 55.3 (C10).

*3-((4-Hydroxyphenoxy)methyl)benzoic acid (*4c*)*

Yellow solid; yield: 30%. ^{1}H NMR (300 MHz, Methanol-d_4) δ (ppm): 8.10 (s, 1H, H2), 7.98 (d, *J* = 7.6 Hz, 1H, H6), 7.67 (d, *J* = 7.5 Hz, 1H, H4), 7.49 (t, *J* = 7.7 Hz, 1H, H5), 6.86 (d, *J* = 8.9 Hz, 2H, H6'-H2'), 6.73 (d, *J* = 8.9 Hz, 2H, H5'-H3'), 5.06 (s, 2H, H7). ^{13}C NMR (75 MHz, Methanol-d_4) δ (ppm): 169.9 (C8), 153.4 (C4'), 152.7 (C1'), 139.7 (C3), 132.42 (C1), 132.9 (C4), 130.0 (C6), 129.7 (C2), 129.6 (C5), 117.2 (C6'-C2'), 116.9 (C5'-C3'), 71.4 (C7).

*3-((4-Nitrophenoxy)methyl)benzoic acid (*4d*)*

Yellow solid; yield: 70%. ^{1}H NMR (300 MHz, D_2O) δ (ppm): 7.99 (d, *J* = 9.1 Hz, 2H, H5'-H3'), 7.89 (s, 1H, H2), 7.81 (d, *J* = 7.3 Hz, 1H, H6), 7.45 (t, *J* = 6.5 Hz, 1H, H5), 7.39 (d, *J* = 7.5 Hz, 1H, H4), 6.94 (d, *J* = 9.1 Hz, 2H, H6'-H2'), 5.10 (s, 2H, H7). ^{13}C NMR (75 MHz, D_2O) δ (ppm): 174.9 (C8), 163.3 (C1'), 141.1 (C4'), 136.9 (C3), 135.7 (C1), 130.3 (C4), 128.9 (C6), 128.7 (C2), 128.3 (C5), 126.7 (C5'-C3'), 115.1 (C6'-C2'), 70.4 (C7).

*3-((Phenylamino)methyl)benzoic acid (*4e*)*

Yellow solid; yield: 64%. ^{1}H NMR (300 MHz, DMSO-d_6) δ (ppm): 7.93 (s, 1H, H2), 7.83 (d, *J* = 6.2 Hz, 1H, H6), 7.41 – 7.38 (m, 2H, H4-H5), 7.06 (t, *J* = 7.4 Hz, 2H, H5'-H3'), 6.65 (d, *J* = 7.9 Hz 2H, H6'-H2'), 6.58 (t, *J* = 7.1 Hz, 1H, H4'), 6.60 (d, *J* = 7.7 Hz, 2H, H6'-H2'), 4.72 (s, 2H, H7), 4.54 (s, 1H, NH). ^{13}C NMR (75 MHz, DMSO-d_6) δ (ppm): 166.5 (C8), 148.1 (C1'), 139.1 (C3), 130.2 (C4), 128.9 (C3'-

575 C5'),128.3 (C6), 127.8 (C1), 127.5 (C2), 128.5 (C5), 116.3 (C4'), 112.5 (C6'-C2'),
576 48.6 (C7).
577
578 *3-((phenylthio)methyl)benzoic acid (*4f*)*
579 White solid; yield: 70%. ^{1}H NMR (300 MHz, DMSO-d_6): δ = 7.95 (s, 1H, H2), 7.81
580 (d, *J* = 7.7 Hz, 1H, H6), 7.58 (d, *J* = 7.6 Hz, 1H, H4), 7.41 (t, *J* = 7.7 Hz, 1H H5),
581 7.34 (d, *J* = 7.1 Hz, 2H, H6'-H2'), 7.29 (t, *J* = 7.5 Hz, 2H, H5'-H3'), 7.18 (t, *J* = 7.0
582 Hz, 1H, H4'), 4.32 (s, 2H, H7). ^{13}C NMR (75 MHz, DMSO-d_6) δ (ppm): 167.0 (C8),
583 147.9 (C1'), 140.1 (C3), 131.9 (C4), 130.6 (C6), 129.3 (C3'-C5'),128.8 (C1), 128.7
584 (C2), 128.5 (C5), 117.8 (C4'), 113.0 (C6'-C2'), 48.0 (C7), 52.1 (C9).
585
586 *3-benzyloxy benzoate (*4g*)*
587 Yellow solid; yield: 80%. ^{1}H NMR (300 MHz, DMSO-d_6) δ (ppm): 13.0 (s, 1H, H9),
588 7.60 – 7.29 (m, 9H), 5.21 (s, 2H, H7). ^{13}C NMR (75 MHz, $CDCl_3$) δ (ppm): 167.0
589 (C8), 158.3 (C3), 136.8 (C1'), 132.2 (C1), 129.7 (C5), 128.4 (C5'-C3'), 127.8 (C1),
590 127.6 (C6'-C2'), 121.8 (C4), 119.7 (C6), 114.9 (C2), 69.3 (C7).
591
592 *4-Phenoxymethyl benzoic acid (*4h*)*
593 White solid; yield: 68%. ^{1}H NMR (300 MHz, DMSO-d_6) δ (ppm): 12.93 (s, 1H,
594 H9), 7.97 (d, *J* = 7.7 Hz, 2H, H6-H2), 7.57 (d, *J* = 7.7 Hz, 2H, H5-H3), 7.30 (t, *J* =
595 7.9 Hz, 1H, H5'-H3'), 7.02 (d, *J* = 7.9 Hz 2H, H6'-H2'), 6.95 (t, *J* = 7.3 Hz, 1H,
596 H4'), 5.19 (s, 2H, H7). ^{13}C NMR (75 MHz, DMSO-d_6) δ (ppm): 167.1 (C8), 158.1
597 (C1'), 142.2 (C4), 130.1 (C6-C2), 129.5 (C5-C3), 127.3 (C5'-C3'), 120.9 (C4'),
598 114.8 (C6'-C2'), 68.5 (C7).
599
600 *4-((4-Methoxyphenoxy)methyl)benzoic acid (*4i*)*
601 White solid; yield: 83%. ^{1}H NMR (300 MHz, DMSO-d_6) δ (ppm): 7.96 (d, *J* = 8.0
602 Hz, 2H, H6-H2), 7.54 (d, *J* = 8.0 Hz, 2H, H5-H3), 6.95 (d, *J* = 9.0 Hz, 2H, H5'-
603 H3'), 6.86 (d, *J* = 9.0 Hz, 2H, H6'-H2'), 5.13 (s, 2H, H7), 3.69 (s, 3H, H10). ^{13}C
604 NMR (75 MHz, DMSO-d_6) δ (ppm): 167.1 (C8), 153.6 (C4'), 152.1 (C1'), 142.4
605 (C4), 130.2 (C5-C3), 127.2 (C6-C2), 115.8 (C6'-C2'), 114.6 (C5'-C3'), 69.1 (C7),
606 55.3 (C10).
607
608 *3-(4-Phenyl-1*H*-1,2,3-triazol-1-yl)benzoic acid (*10a*)*

Yellow solid; yield: 90%. ^{1}H NMR (300 MHz, Methanol-d_4) δ (ppm): 8.80 (s, 1H, H8), 8.35 (s, 1H, H2) 7.99 (d, *J* = 7.7 Hz, 1H, H6), 7.91 (d, *J* = 7.1 Hz, 1H, H4), 7.83 (d, *J* = 8.1 Hz, 2H, H6'-H3'), 7.52 (t, *J* = 7.9 Hz, 1H, H5), 7.36 (t, *J* = 7.6 Hz, 2H, H5'-H3'), 7.27 (t, *J* = 7.3 Hz, 1H, H4'). ^{13}C NMR (75 MHz, Methanol-d_4) δ (ppm): 172.3 (C9), 149.7 (C7), 140.0 (C3), 138.2 (C1), 131.5 (C1'), 130.8 (C5), 130.6 (C4'), 130.0 (C3'-C5'), 129.6 (C4), 126.8 (C2'-C6'), 123.6 (C8), 122.2 (C2).

*3-(4-(Phenoxymethyl)-1*H*-1,2,3-triazol-1-yl) benzoic acid (*10b*)*

Yellow solid; yield: 98%. ^{1}H NMR (300 MHz, Methanol-d_4) δ (ppm): 8.63 (s, 1H, H9), 8.40 (s, 1H, H2), 8.10 (d, *J* = 7.6 Hz, 1H, H6), 7.95 (d, *J* = 8.0 Hz, 1H, H4), 7.61 (t, *J* = 7.9 Hz, 1H, H5), 7.31 (t, *J* = 7.4 Hz, 2H, H5'-H3'), 7.06 (d, *J* = 8.0 Hz, 2H, H6'-H2'), 6.97 (t, *J* = 7.3 Hz, 1H, H4'), 5.27 (s, 2H, H7). ^{13}C NMR (75 MHz, Methanol-d_4) δ (ppm): 172.5 (C10), 159.8 (C1), 146.1 (C8), 140.1 (C3), 138.1 (C1), 130.8 (C5), 130.6 (C3'-C5'), 123.7 (C2), 123.6 (C4'), 122.8 (C9), 116.0 (C2'-C6'), 62.4 (C7).

4.2.3 Synthesis of tetrazoles (7)

Methyl 3-(4-phenyl-1*H*-1,2,3-triazol-1-yl)benzoate was dissolved in DMF (4 mL/mmol) and then NaN_3 (1.2 eq.) and NH_4Cl (1.2 eq.) were added. The mixture was maintained under stirring and reflux for 16 hours. Afterward, water was added and the mixture was washed with EtOAc. Lastly, the pH of the aqueous phase was adjusted to 1.00 with the addition of 5% (v/v) HCl solution and the mixture was kept under stirring for 30 minutes. The precipitate was filtered and washed with water [37].

5-(3-(phenoxymethyl)phenyl)-1H-tetrazole (7)

Yellow solid; yield: 5%. ^{1}H NMR (300 MHz, Methanol-d_4) δ (ppm): 8.03 (s, 1H, H2), 7.87 (d, *J* = 7.5 Hz, 1H, H6), 7.56 (d, *J* = 7.7 Hz, 1H, H4), 7.49 (t, *J* = 7.6 Hz, 1H, H5), 7.18 (t, *J* = 7.9 Hz, 2H, H5'-H3'), 6.62 (d, *J* = 8.0 Hz, 2H, H2'-H6') 6.84 (t, *J* = 7.3 Hz, 1H, H4'), 5.07 (s, 2H, H7). ^{13}C NMR (75 MHz, Methanol-d_4) δ (ppm): 160.1 (C1'), 157.5 (C8), 140.6 (C3), 131.0 (C4), 130.7 (C6), 130.6 (C5'-C3'), 127.6 (C5), 127.1 (C4), 125.7 (C1), 122.2 (C4'), 116.0 (C6'-C2'), 70.2 (C7).

4.3 Molecular modeling and molecular dynamics simulation

The PDB structure of *Mt*DHFR co-crystallized with dihydrofolate substrate (DHF, PDB ID: 6NND) and the antifolates methotrexate (MTX, 1DF7), with pemetrexed (PMX, 6NNC) and diaverdine (DIA, 6NNE) were selected for simulation, as well as the structure with only NADPH (1DG8). A single chain as a monomer was selected for each of the structures for molecular modelling, based on the number of Ramachandran outliers. The Small-Molecule Drug Discovery Suite (v2019.3, Schrödinger, LLC, New York, NY, 2019) was used for all calculations. Protein structures were prepared by adding hydrogen atoms and fixing missing sidechains using the Protein Preparation Wizard (PrepWiz) [38], missing loops were generated using Prime and sulfate/crystallization buffer molecules, such as glycerol (GOL) were removed. Asp27 ionization state as well as the ligand N3, and equivalent in other ligands, were assigned according to the experimental results from Wan *et al.*, 2014, where the folate N3 atom established an ionic interaction with the negatively charged Asp27 [39].

Molecular docking of chosen ligands from our series (4b, 4e and 4h) was performed in a grid encompassing residues around 20 Å from the centroid of the co-crystallized ligand, using the default settings of the Glide program (Glide v7.7, Maestro v2019.3) in extra-precision mode, with at least five poses selected for further visual inspection [40]. Amino acid residues were considered rigid and both structural water molecules and cofactor NAD^+ were maintained in the active site during the calculation.

Protein complexes with the original co-crystallized ligands and with the docked ligands were submitted for molecular dynamics simulations (MD) in order to evaluate both the ligand stability and the effects of ligand-binding upon the protein (the full protocol was previously described [41]. MD simulations were carried out using Desmond [42], with the OPLS3e force-field [43]. The simulated system encompassed the protein-ligand complexes, a predefined water model (TIP3P [44]) as a solvent and counterions (Na^+ or Cl^- adjusted to neutralize the overall system charge). The system was treated in a cubic box with periodic boundary conditions specifying the shape and the size of the box as 13 Å distance from the box edges to any atom of the protein. We used a time step of 1 fs, the short-range coulombic interactions were treated using a cut-off value of 9.0 Å using the short-range method, while the smooth Particle Mesh Ewald method (PME) handled long-range coulombic interactions [45].

Initially, the relaxation of the system was performed using Steepest Descent and the limited-memory Broyden-Fletcher-Goldfarb-Shanno algorithms in a hybrid manner. The simulation was performed under the NPT ensemble for 5 ns implementing the Berendsen thermostat and barostat methods. A constant temperature of 310 K was maintained throughout the simulation using the Nose-Hoover thermostat algorithm and Martyna-Tobias-Klein Barostat algorithm to maintain 1 atm of pressure, respectively.

After minimization and relaxation of the system, we proceeded with a single production step of at least 1 μs, with sampling every 500 ps. The representative structure was selected by inspecting changes in the Root-mean-square deviation (RMSD, Supplementary Data, where Figure 2 represents the variation of the RMSD values along with the simulation and the changes in the RMSF values, Root-mean-square fluctuation, by residue for the protein backbone, on Figure 3). Interactions and distances were determined using the Simulation Event Analysis pipeline implemented in Maestro (Maestro v2019.3). The current geometric criteria for protein-ligand hydrogen bond is a distance of 2.5 Å between the donor and acceptor atoms (D — H···A); a donor angle of ≥120° between the donor-hydrogen-acceptor atoms (D — H···A); and an acceptor angle of ≥90° between the hydrogen-acceptor-bonded atom atoms (H···A — X). Similarly, protein-water or water-ligand hydrogen bond had a distance of 2.8 Å between the donor and acceptor atoms (D—H···A); a donor angle of ≥110° between the donor-hydrogen-acceptor atoms (D—H···A); and an acceptor angle of ≥90° between the hydrogen-acceptor-bonded atom atoms (H···A—X). Non-specific hydrophobic interactions are defined by hydrophobic sidechain within 3.6 Å of a ligand's aromatic or aliphatic carbons and π-π interactions required two aromatic groups stacked face-to-face or face-to-edge, within 4.5 Å of distance. Trajectories and interaction data are available on Zenodo repository (under the code: 10.5281/zenodo.3663046).

Conflict of interest

Authors declare no conflict of interest

Acknowledgments

The authors are grateful to CAPES, CNPq (grant number 153232/2018-8, 436791/2018-8 and 310232/2017-1) and FAPESP (grant numbers 2013/15906-5, 2013/18160-4, 2017/00689-0 and 2017/25543-8) for financial support. The authors wish to acknowledge the CSC – IT Center for Science, Finland, for the generous computational resources.

References

[1] M. Pai, M.A. Behr, D. Dowdy, K. Dheda, M. Divangahi, C.C. Boehme, A. Ginsberg, S. Swaminathan, M. Spigelman, H. Getahun, D. Menzies, M. Raviglione, Tuberculosis, Nature Reviews Disease Primers. 2 (2016) 16076. https://doi.org/10.1038/nrdp.2016.76.

[2] WHO, WHO | Global tuberculosis report 2019, WHO. (2019).

[3] C.M.A. Pinto, A.R.M. Carvalho, New findings on the dynamics of HIV and TB coinfection models, Applied Mathematics and Computation. 242 (2014) 36–46. https://doi.org/10.1016/j.amc.2014.05.061.

[4] A.I. Zumla, S.H. Gillespie, M. Hoelscher, P.P.J. Philips, S.T. Cole, I. Abubakar, T.D. McHugh, M. Schito, M. Maeurer, A.J. Nunn, New antituberculosis drugs, regimens, and adjunct therapies: needs, advances, and future prospects, The Lancet Infectious Diseases. 14 (2014) 327–340. https://doi.org/10.1016/S1473-3099(13)70328-1.

[5] E. Martinez, D. Hennessy, P. Jelfs, T. Crighton, S.C.-A. Chen, V. Sintchenko, Mutations associated with in vitro resistance to bedaquiline in Mycobacterium tuberculosis isolates in Australia, Tuberculosis. 111 (2018) 31–34. https://doi.org/10.1016/j.tube.2018.04.007.

[6] N. Veziris, C. Bernard, L. Guglielmetti, D. Le Du, D. Marigot-Outtandy, M. Jaspard, E. Caumes, I. Lerat, C. Rioux, Y. Yazdanpanah, A. Tiotiu, N. Lemaitre, F. Brossier, V. Jarlier, J. Robert, W. Sougakoff, A. Aubry, CNR MyRMA and the Tuberculosis Consilium of the CNR MyRMA, CNR MyRMA and Tuberculosis Consilium of the CNR MyRMA, Rapid emergence of *Mycobacterium tuberculosis* bedaquiline resistance: lessons to avoid repeating past errors, European Respiratory Journal. 49 (2017) 1601719. https://doi.org/10.1183/13993003.01719-2016.

[7] A.D. Hanson, J.F. Gregory, Folate Biosynthesis, Turnover, and Transport in Plants, Annual Review of Plant Biology. 62 (2011) 105–125. https://doi.org/10.1146/annurev-arplant-042110-103819.

[8] A. Bermingham, J.P. Derrick, The folic acid biosynthesis pathway in bacteria: evaluation of potential for antibacterial drug discovery, BioEssays. 24 (2002) 637–648. https://doi.org/10.1002/bies.10114.

[9] I. Hershkovitz, H.D. Donoghue, D.E. Minnikin, G.S. Besra, O.Y.-C. Lee, A.M. Gernaey, E. Galili, V. Eshed, C.L. Greenblatt, E. Lemma, G.K. Bar-Gal, M. Spigelman, Detection and Molecular Characterization of 9000-Year-Old Mycobacterium tuberculosis from a Neolithic Settlement in the Eastern Mediterranean, PLoS ONE. 3 (2008) e3426. https://doi.org/10.1371/journal.pone.0003426.

[10] Y. Liu, X. Zhang, Y. Zhang, Y. Sun, C. Yao, W. Wang, C. Li, Characterization of Mycobacterium tuberculosis strains in Beijing, China: drug susceptibility

phenotypes and Beijing genotype family transmission, BMC Infectious Diseases. 18 (2018) 658. https://doi.org/10.1186/s12879-018-3578-7.

[11] G. Bhabha, D.C. Ekiert, M. Jennewein, C.M. Zmasek, L.M. Tuttle, G. Kroon, H.J. Dyson, A. Godzik, I.A. Wilson, P.E. Wright, Divergent evolution of protein conformational dynamics in dihydrofolate reductase, Nature Structural & Molecular Biology. 20 (2013) 1243–1249. https://doi.org/10.1038/nsmb.2676.

[12] W. Hong, Y. Wang, Z. Chang, Y. Yang, J. Pu, T. Sun, S. Kaur, J.C. Sacchettini, H. Jung, W. Lin Wong, L. Fah Yap, Y. Fong Ngeow, I.C. Paterson, H. Wang, The identification of novel Mycobacterium tuberculosis DHFR inhibitors and the investigation of their binding preferences by using molecular modelling, Scientific Reports. 5 (2015) 15328. https://doi.org/10.1038/srep15328.

[13] A.B. Gerum, J.E. Ulmer, D.P. Jacobus, N.P. Jensen, D.R. Sherman, C.H. Sibley, Novel Saccharomyces cerevisiae screen identifies WR99210 analogues that inhibit Mycobacterium tuberculosis dihydrofolate reductase., Antimicrobial Agents and Chemotherapy. 46 (2002) 3362–9. https://doi.org/10.1128/aac.46.11.3362-3369.2002.

[14] M.V.B. Dias, P. Tyrakis, R.R. Domingues, A.F. Paes Leme, T.L. Blundell, Mycobacterium tuberculosis dihydrofolate reductase reveals two conformational states and a possible low affinity mechanism to antifolate drugs, Structure. 22 (2014) 94–103. https://doi.org/10.1016/j.str.2013.09.022.

[15] R. Li, R. Sirawaraporn, P. Chitnumsub, W. Sirawaraporn, J. Wooden, F. Athappilly, S. Turley, W.G.J. Hol, Three-dimensional structure of M. tuberculosis dihydrofolate reductase reveals opportunities for the design of novel tuberculosis drugs, Journal of Molecular Biology. 295 (2000) 307–323. https://doi.org/10.1006/jmbi.1999.3328.

[16] S.Z. Wiktor, M. Sassan-Morokro, A.D. Grant, L. Abouya, J.M. Karon, C. Maurice, G. Djomand, A. Ackah, K. Domoua, A. Kadio, A. Yapi, P. Combe, O. Tossou, T.H. Roels, E.M. Lackritz, D. Coulibaly, K.M. De Cock, I.M. Coulibaly, A.E. Greenberg, Efficacy of trimethoprim-sulphamethoxazole prophylaxis to decrease morbidity and mortality in HIV-1-infected patients with tuberculosis in Abidjan, Côte d'Ivoire: a randomised controlled trial., Lancet (London, England). 353 (1999) 1469–75. https://doi.org/10.1016/s0140-6736(99)03465-0.

[17] X. Yang, W. Wedajo, Y. Yamada, S.-L. Dahlroth, J.J.-L. Neo, T. Dick, W.-K. Chui, 1,3,5-triazaspiro[5.5]undeca-2,4-dienes as selective Mycobacterium tuberculosis dihydrofolate reductase inhibitors with potent whole cell activity, European Journal of Medicinal Chemistry. 144 (2018) 262–276. https://doi.org/10.1016/j.ejmech.2017.12.017.

[18] M.H.R.I. El-Hamamsy, A.W. Smith, A.S. Thompson, M.D. Threadgill, Structure-based design, synthesis and preliminary evaluation of selective inhibitors of dihydrofolate reductase from Mycobacterium tuberculosis, Bioorganic & Medicinal Chemistry. 15 (2007) 4552–4576. https://doi.org/10.1016/j.bmc.2007.04.011.

[19] N.R. Tawari, S. Bag, A. Raju, A.C. Lele, R. Bairwa, M.K. Ray, M. Rajan, L.U. Nawale, D. Sarkar, M.S. Degani, Rational drug design, synthesis and biological evaluation of dihydrofolate reductase inhibitors as antituberculosis

agents, Future Medicinal Chemistry. 7 (2015) 979–988. https://doi.org/10.4155/fmc.15.48.

[20] A.W. Schüttelkopf, L.W. Hardy, S.M. Beverley, W.N. Hunter, Structures of Leishmania major pteridine reductase complexes reveal the active site features important for ligand binding and to guide inhibitor design., Journal of Molecular Biology. 352 (2005) 105–16. https://doi.org/10.1016/j.jmb.2005.06.076.

[21] I.O. Donkor, H. Li, S.F. Queener, Synthesis and DHFR inhibitory activity of a series of 6-substituted-2,4-diaminothieno[2,3-d]pyrimidines., European Journal of Medicinal Chemistry. 38 (2003) 605–11. https://doi.org/10.1016/S0223-5234(03)00101-6.

[22] S. Singh, B.K. Malik, D.K. Sharma, Molecular drug targets and structure based drug design: A holistic approach, Bioinformation. 1 (2006) 314–320.

[23] C. Vilchèze, W.R. Jacobs, The combination of sulfamethoxazole, trimethoprim, and isoniazid or rifampin is bactericidal and prevents the emergence of drug resistance in Mycobacterium tuberculosis, Antimicrobial Agents and Chemotherapy. 56 (2012) 5142–5148. https://doi.org/10.1128/AAC.00832-12.

[24] R.L. Then, Antimicrobial dihydrofolate reductase inhibitors--achievements and future options: review, J Chemother. 16 (2004) 3–12. https://doi.org/10.1179/joc.2004.16.1.3.

[25] J.A. Ribeiro, A. Hammer, G.A. Libreros Zúñiga, S.M. Chavez-Pacheco, P. Tyrakis, G.S. de Oliveira, T. Kirkman, J.E. Bakali, S.A. Rocco, M.L. Sforça, R. Parise-Filho, A.G. Coyne, T.L. Blundell, C. Abell, M.V. Bertacine Dias, Using a fragment-based approach to identify novel chemical scaffolds targeting the dihydrofolate reductase (DHFR) from Mycobacterium tuberculosis, BioRxiv. (2020) 2020.03.30.016204. https://doi.org/10.1101/2020.03.30.016204.

[26] J.A. Ribeiro, S.M. Chavez-Pacheco, G.S. de Oliveira, C. dos S. Silva, J.H.P. Giudice, G.A. Libreros-Zúñiga, M.V.B. Dias, Crystal structures of the closed form of *Mycobacterium tuberculosis* dihydrofolate reductase in complex with dihydrofolate and antifolates, Acta Crystallographica Section D Structural Biology. 75 (2019) 682–693. https://doi.org/10.1107/S205979831900901X.

[27] O. Rimet, M. Chauvet, M. Bourdeaux, C. Briand, A novel fluorometric assay for quantitative analysis of dihydrofolate reductase activity in biological samples., Journal of Biochemical and Biophysical Methods. 14 (1987) 335–42. https://doi.org/10.1016/0165-022x(87)90027-3.

[28] H. Masuoka, K. Fujimori, S. Sekiguchi, M. Watanabe, H. Wang, T. Aiso, H. Yamaya, A. Satoh, S. Satomi, Beneficial effect of FR183998, a Na+/H+ exchanger inhibitor, on porcine pancreas allotransplantation retrieved from non-heart-beating donors, Transplant Proc. 37 (2005) 223–225. https://doi.org/10.1016/j.transproceed.2004.12.227.

[29] M.R. Sawaya, J. Kraut, Loop and Subdomain Movements in the Mechanism of *Escherichia coli* Dihydrofolate Reductase: Crystallographic Evidence † , ‡, Biochemistry. 36 (1997) 586–603. https://doi.org/10.1021/bi962337c.

[30] R.A. Copeland, Evaluation of Enzyme Inhibitors in Drug Discovery, John Wiley & Sons, Inc., Hoboken, NJ, USA, 2013. https://doi.org/10.1002/9781118540398.

[31] B. Srinivasan, J. V. Rodrigues, S. Tonddast-Navaei, E. Shakhnovich, J. Skolnick, Rational Design of Novel Allosteric Dihydrofolate Reductase

Inhibitors Showing Antibacterial Effects on Drug-Resistant *Escherichia coli* Escape Variants, ACS Chemical Biology. 12 (2017) 1848–1857. https://doi.org/10.1021/acschembio.7b00175.

[32] K.M. Frey, J. Liu, M.N. Lombardo, D.B. Bolstad, D.L. Wright, A.C. Anderson, Crystal structures of wild-type and mutant methicillin-resistant Staphylococcus aureus dihydrofolate reductase reveal an alternate conformation of NADPH that may be linked to trimethoprim resistance., Journal of Molecular Biology. 387 (2009) 1298–308. https://doi.org/10.1016/j.jmb.2009.02.045.

[33] T.D. Meek, E.P. Garvey, D. V. Santi, Purification and characterization of the bifunctional thymidylate synthetase-dihydrofolate reductase from methotrexate-resistant Leishmania tropica, Biochemistry. 24 (1985) 678–686. https://doi.org/10.1021/bi00324a021.

[34] A. Manos-Turvey, E.M.M. Bulloch, P.J. Rutledge, E.N. Baker, J.S. Lott, R.J. Payne, Inhibition Studies of Mycobacterium tuberculosis Salicylate Synthase (MbtI), ChemMedChem. 5 (2010) 1067–1079. https://doi.org/10.1002/cmdc.201000137.

[35] K. Kutonova, M. Trusova, P. Postnikov, V. Filimonov, J. Parello, A Simple and Effective Synthesis of Aryl Azides via Arenediazonium Tosylates, Synthesis. 45 (2013) 2706–2710. https://doi.org/10.1055/s-0033-1339648.

[36] X.-J. Wang, P.-Z. Li, L. Liu, Q. Zhang, P. Borah, J.D. Wong, X.X. Chan, G. Rakesh, Y. Li, Y. Zhao, Significant gas uptake enhancement by post-exchange of zinc(ii) with copper(ii) within a metal–organic framework, Chemical Communications. 48 (2012) 10286. https://doi.org/10.1039/c2cc34921c.

[37] S. Vorona, T. Artamonova, Y. Zevatskii, L. Myznikov, An Improved Protocol for the Preparation of 5-Substituted Tetrazoles from Organic Thiocyanates and Nitriles, Synthesis. 46 (2014) 781–786. https://doi.org/10.1055/s-0033-1340616.

[38] G. Madhavi Sastry, M. Adzhigirey, T. Day, R. Annabhimoju, W. Sherman, Protein and ligand preparation: parameters, protocols, and influence on virtual screening enrichments, Journal of Computer-Aided Molecular Design. 27 (2013) 221–234. https://doi.org/10.1007/s10822-013-9644-8.

[39] Q. Wan, B.C. Bennett, M.A. Wilson, A. Kovalevsky, P. Langan, E.E. Howell, C. Dealwis, Toward resolving the catalytic mechanism of dihydrofolate reductase using neutron and ultrahigh-resolution X-ray crystallography, Proceedings of the National Academy of Sciences. 111 (2014) 18225–18230. https://doi.org/10.1073/pnas.1415856111.

[40] R.A. Friesner, R.B. Murphy, M.P. Repasky, L.L. Frye, J.R. Greenwood, T.A. Halgren, P.C. Sanschagrin, D.T. Mainz, Extra Precision Glide: Docking and Scoring Incorporating a Model of Hydrophobic Enclosure for Protein−Ligand Complexes, Journal of Medicinal Chemistry. 49 (2006) 6177–6196. https://doi.org/10.1021/jm051256o.

[41] T. Kronenberger, P. Oliveira Fernades, I. Drumond Franco, A. Poso, V. Gonçalves Maltarollo, Ligand- and Structure-Based Approaches of *Escherichia coli* FabI Inhibition by Triclosan Derivatives: From Chemical Similarity to Protein Dynamics Influence, ChemMedChem. (2019) cmdc.201900415. https://doi.org/10.1002/cmdc.201900415.

[42] R.O. Dror, M.Ø. Jensen, D.W. Borhani, D.E. Shaw, Exploring atomic resolution physiology on a femtosecond to millisecond timescale using

molecular dynamics simulations., The Journal of General Physiology. 135 (2010) 555–62. https://doi.org/10.1085/jgp.200910373.
[43] E. Harder, W. Damm, J. Maple, C. Wu, M. Reboul, J.Y. Xiang, L. Wang, D. Lupyan, M.K. Dahlgren, J.L. Knight, J.W. Kaus, D.S. Cerutti, G. Krilov, W.L. Jorgensen, R. Abel, R.A. Friesner, OPLS3: A Force Field Providing Broad Coverage of Drug-like Small Molecules and Proteins, Journal of Chemical Theory and Computation. 12 (2016) 281–296. https://doi.org/10.1021/acs.jctc.5b00864.
[44] W.L. Jorgensen, J. Chandrasekhar, J.D. Madura, R.W. Impey, M.L. Klein, Comparison of simple potential functions for simulating liquid water, The Journal of Chemical Physics. 79 (1983) 926–935. https://doi.org/10.1063/1.445869.
[45] T. Darden, D. York, L. Pedersen, Particle mesh Ewald: An $N \cdot \log(N)$ method for Ewald sums in large systems, The Journal of Chemical Physics. 98 (1993) 10089–10092. https://doi.org/10.1063/1.464397.

UNIVERSITY OF SAO PAULO

Faculty of Pharmaceutical Sciences

Department of Pharmacy

February 20th, 2020

Professor F. Romesberg
The Scripps Research Institute

Dear Editor,

We wish to confirm that there are no known conflicts of interest associated with this publication and there has been no significant financial support for this work that could have influenced its outcome. We confirm that the manuscript has been read and approved by all named authors and that there are no other persons who satisfied the criteria for authorship but are not listed. We further confirm that the order of authors listed in the manuscript has been approved by all of us. We confirm that we have given due consideration to the protection of intellectual property associated with this work and that there are no impediments to publication, including the timing of publication, with respect to intellectual property. In so doing we confirm that we have followed the regulations of our institutions concerning intellectual property. We understand that the Corresponding Author is the sole contact for the Editorial process (including Editorial Manager and direct communications with the office). He/she is responsible for communicating with the other authors about progress, submissions of revisions and final approval of proofs. We confirm that we have provided a current, correct email address which is accessible by the Corresponding Author and which has been configured to accept email from (roberto.parise@usp.br). All authors have approved the manuscript and agree with its submission.

Sincerely yours,

Roberto Parise Filho, Ph.D. (on behalf of the authors)
Assistant Professor
Laboratory of Design and Synthesis of Bioactive Substances (LAPESSB)

University of Sao Paulo
E-mail: roberto.parise@usp.br

Authors: Thales Kronenberger, Glaucio Monteiro Ferreira, Alfredo Danilo Ferreira de Souza, Soraya da Silva Santos, Antti Poso, João Augusto Ribeiro, Maurício Temotheo Tavares, Fernando Rogério Pavan, Gustavo Henrique Goulart Trossini, Marcio Vinícius Bertacine Dias, Roberto Parise-Filho